LETTERS

# High-*Q* surface-plasmon-polariton whispering-gallery microcavity

Bumki Min[1,2]†, Eric Ostby[1], Volker Sorger[2], Erick Ulin-Avila[2], Lan Yang[1]†, Xiang Zhang[2,3] & Kerry Vahala[1]

**Surface plasmon polaritons (SPPs) are electron density waves excited at the interfaces between metals and dielectric materials[1]. Owing to their highly localized electromagnetic fields, they may be used for the transport and manipulation of photons on subwavelength scales[2–9]. In particular, plasmonic resonant cavities represent an application that could exploit this field compression to create ultra-small-mode-volume devices. A key figure of merit in this regard is the ratio of cavity quality factor, *Q* (related to the dissipation rate of photons confined to the cavity), to cavity mode volume, *V* (refs 10, 11). However, plasmonic cavity *Q* factors have so far been limited to values less than 100 both for visible and near-infrared wavelengths[12–16]. Significantly, such values are far below the theoretically achievable *Q* factors for plasmonic resonant structures. Here we demonstrate a high-*Q* SPP whispering-gallery microcavity that is made by coating the surface of a high-*Q* silica microresonator with a thin layer of a noble metal. Using this structure, *Q* factors of 1,376 ± 65 can be achieved in the near infrared for surface-plasmonic whispering-gallery modes at room temperature. This nearly ideal value, which is close to the theoretical metal-loss-limited *Q* factor, is attributed to the suppression and minimization of radiation and scattering losses that are made possible by the geometrical structure and the fabrication method. The SPP eigenmodes, as well as the dielectric eigenmodes, are confined within the whispering-gallery microcavity and accessed evanescently using a single strand of low-loss, tapered optical waveguide[17,18]. This coupling scheme provides a convenient way of selectively exciting and probing confined SPP eigenmodes. Up to 49.7 per cent of input power is coupled by phase-matching control between the microcavity SPP and the tapered fibre eigenmodes.**

The subject of high-*Q* optical micro- and nanocavities has been intensively investigated over the last decade. The extremely low photon loss rate and small cavity mode volume of photonic-crystal or whispering-gallery devices offer surprisingly rich physics, spanning many areas of research including nonlinear optics, quantum optics, and device physics[10,11]. Whereas optical micro- and nanocavities made of dielectric or semiconducting materials exhibit large *Q* factors as well as small diffraction-limited cavity mode volumes, their metallic counterparts (surface-plasmonic cavities[12–16]) have been optimized primarily for subwavelength-scale miniaturization and have given results well below the theoretically predicted performance limit—especially in terms of cavity loss—set by ohmic loss in the metal. This is believed to result from other loss contributions such as surface scattering, radiation, finite cavity mirror reflectance or a significant degree of field penetration into the metal. However, these seemingly distinct dielectric and plasmonic waveguiding principles can be combined in a single cavity by using mature optical microcavity technology such as that provided by disk[19,20] or toroidal microcavities[21]. Here we propose to utilize a dielectric microcavity, engineered to minimize surface blemishes and thereby reduce scattering[19,20], as a template for the creation of a surface-plasmonic whispering-gallery microcavity with a cavity plasmon-polariton loss rate close to the theoretical limit.

The proposed plasmonic microdisk cavity structure is sketched in Fig. 1a. The plasmonic cavity is composed of a core silica (silicon dioxide) disk microcavity clad in a thin layer of silver (see Methods). Silica microdisk resonators are ideal templates for the study of surface-plasmonic whispering-gallery modes primarily because they routinely have optical *Q* factors greater than 1,000,000 (considerably larger than the metal-loss-limited *Q* factor). Using the wedge structure shown in Fig. 1a, *Q* factors as high as $6 \times 10^7$ have been demonstrated, showing a remarkably low scattering loss value[19]. A scanning electron micrograph of a silver-coated SPP microdisk resonator is shown in Fig. 1b, and the corresponding expanded view of the edge of the disk resonator is shown in Fig. 1c.

A full vectorial finite-element analysis was performed for the SPP microdisk resonators[22,23], taking into account the effects of silver[24] and silica[25] material dispersion. The theoretical cavity mode dispersion diagram of an SPP microdisk resonator (Fig. 2a) shows the real part of the eigenfrequency, $f$, of the cavity modes as a function of an azimuthal mode number, $m$. The vacuum light line is defined by $f = mc/2\pi R_b$ with respect to the bottom radius, $R_b$, of the template silica disk microcavity, and the silica light line is similarly defined by $f = mc/2\pi n_{silica}(f)R_b$. Here $c$ is the speed of light and $n_{silica}$ is the refractive index of silica. The eigenmodes of an SPP microcavity can be classified into two distinctive categories in terms of the cavity mode dispersion: (1) surface-plasmonic modes at the metal–dielectric interface and (2) optical dielectric modes due to the presence of a dielectric waveguiding channel.

In the insets of Fig. 2a, the fundamental (first-order) SPP eigenmode, the second-order SPP eigenmode and the fundamental dielectric eigenmode are plotted for magnetic energy density $u_M = (1/2\mu_0)|\mathbf{B}(r,\phi,z)|^2$ (where $\mu_0$ is the permeability of free space) using a false-colour map (a conventional cylindrical coordinate system $(r,\phi,z)$ is used for the analysis). The SPP eigenmodes of an SPP microdisk resonator have electromagnetic energy-density profiles that peak at the silica–metal interface in the transverse plane (constant $\phi$). The SPP eigenmodes are categorized as $\mathrm{SPP}_{qm}$, where $q$ is the plasmonic mode number ($\mathbf{H}(r,\phi,z) = \mathbf{H}_{\mathrm{SPP}}^{qm}(r,z)e^{im\phi}$), and the optical dielectric eigenmodes are denoted by $\mathrm{DE}_{hm}$, where $h$ is the dielectric mode number ($\mathbf{H}(r,\phi,z) = \mathbf{H}_{\mathrm{DE}}^{hm}(r,z)e^{im\phi}$). The plasmonic mode number is defined as the number of antinodes in $|\mathbf{H}_{\mathrm{SPP}}^{qm}|$ along the silica–metal interface (excluding the vicinity of the sharp corner of the microcavity). Dispersion relations for the four lowest-order SPP eigenmodes ($q = 1, 2, 3, 4$) and the two lowest-order dielectric eigenmodes ($h = 1, 2$; see Methods) are plotted in Fig. 2a.

The cavity mode index, $n_c$, of a specific eigenmode can be evaluated with respect to the dielectric cavity edge ($r = R_b$) as $n_c = mc/2\pi R_b f$.

[1]Thomas J. Watson Laboratory of Applied Physics, California Institute of Technology, Pasadena, California 91125, USA. [2]Nanoscale Science and Engineering Center, 5130 Etcheverry Hall, University of California, Berkeley, California 94720, USA. [3]Material Sciences Division, Lawrence Berkeley National Laboratory, Berkeley, California 94720, USA. †Present addresses: Department of Mechanical Engineering, Korea Advanced Institute of Science and Technology, Daejeon 305-751, Republic of Korea (B.M.); Department of Electrical and Systems Engineering, Washington University in St Louis, St Louis, Missouri 63130, USA (L.Y.).

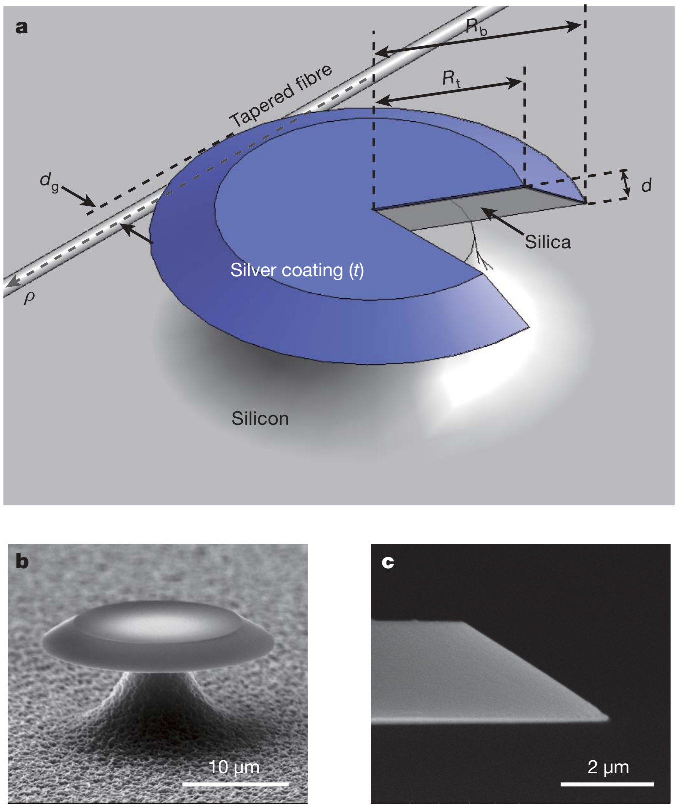


**Figure 1 | Tapered fibre waveguide and SPP whispering-gallery microdisk resonator.** **a**, SPP microdisk resonator with a tapered optical fibre passing under its edge. The wedge-shaped disk edge is a by-product of isotropic buffered hydrofluoric acid etching of silica. A transverse cross-section of the cavity is shown for clarity. $R_b$, bottom radius; $R_t$, top radius; $d$, thickness of the silica disk resonator; $t$, thickness of the metal layer. The straight fibre waveguide axis is denoted by the coordinate $\rho$ and the gap width, $d_g$, is defined as the horizontal distance from the dielectric cavity edge to the fibre axis. **b**, Scanning electron micrograph of a fabricated silver-coated SPP microdisk resonator ($R_b = 10.96$ μm, $R_t = 7.89$ μm, $d = 2$ μm, $t \approx 100$ nm). **c**, Expanded view of the edge of the SPP microdisk resonator.

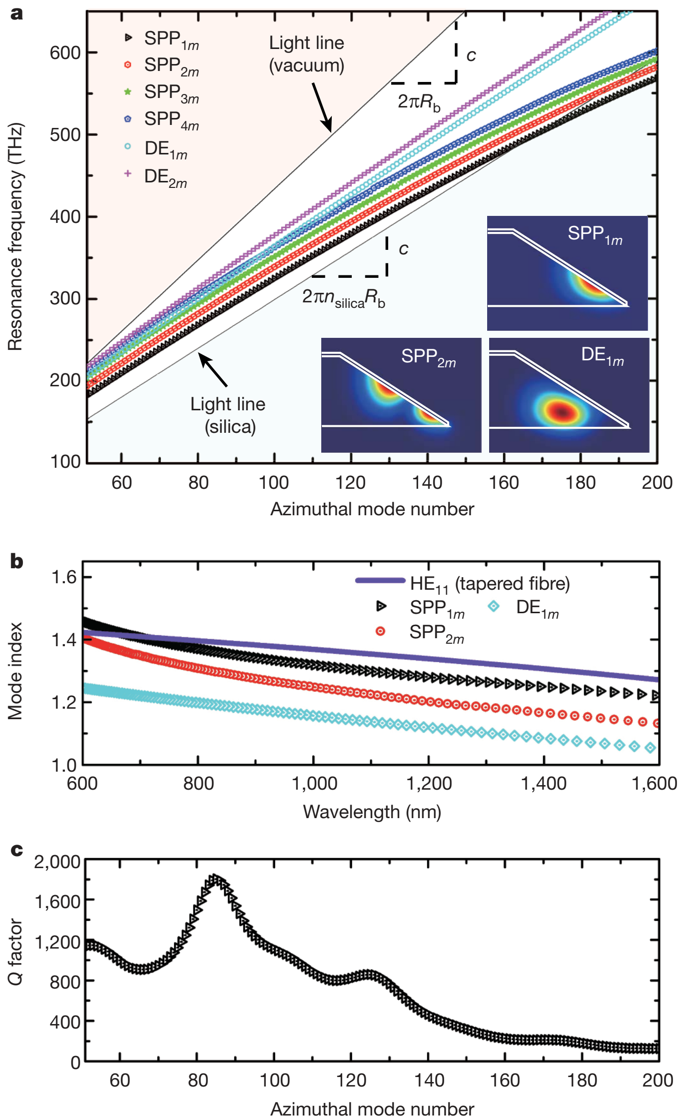


**Figure 2 | Cavity mode dispersion, effective mode index and Q factor.** **a**, Cavity mode dispersion curves for an SPP microdisk resonator, calculated from finite-element eigenfrequency analysis. For this calculation, the thickness of the silver layer is 100 nm, and the bottom and top radii and the thickness of the template silica microdisk resonator were set to 11, 7.9 and 2 μm, respectively. Light lines, corresponding to vacuum and silica, are given as two black lines (silica material dispersion has been taken into account). For clarity, only the four lowest-order SPP eigenmodes and the two lowest-order dielectric eigenmodes are plotted. The first- and second-order SPP eigenmodes (SPP$_{1m}$, SPP$_{2m}$) and the fundamental dielectric eigenmode (DE$_{1m}$) are shown in the inset. **b**, Effective cavity mode indices, $n_c$, of SPP$_{1m}$, SPP$_{2m}$ and DE$_{1m}$ (with respect to $R_b$), shown as a function of resonance wavelength. The mode index of a tapered-fibre HE$_{11}$ mode is shown to demonstrate phase matching. **c**, The theoretical $Q$ factor for SPP$_{1m}$, plotted as a function of azimuthal mode number, $m$.

Figure 2b shows the calculated mode index for modes SPP$_{1m}$, SPP$_{2m}$ and DE$_{1m}$. The mode index of a fundamental surface-plasmonic mode (SPP$_{1m}$) is clearly larger than that of a fundamental dielectric mode (DE$_{1m}$) within most of the visible and near-infrared frequency band, owing to the plasmonic surface-wave characteristics. The mode index is important because it determines the phase-matching condition for excitation of SPP modes by an input tapered fibre waveguide. After $n_c$ has been calculated, the corresponding phase-matched fibre-waveguide mode index can be approximated as

$$n_w \approx n_c \frac{\sin^{-1}\sqrt{\delta(2-\delta)}}{\sqrt{\delta(2-\delta)}} = n_c\left(1+\frac{1}{3}\delta+\frac{2}{15}\delta^2+O(\delta^3)\right) \quad (1)$$

where $\delta = -d_g/R_b \geq 0$ denotes the relative gap width ($d_g$, gap width; see Methods). To qualitatively describe the effect of gap width variation on the phase matching, the HE$_{11}$ mode index of a fibre waveguide with a 1-μm waist diameter is shown in Fig. 2b. The fibre mode index is slightly larger than the SPP$_{1m}$ mode index in the near-infrared wavelength band. However, owing to the above phase-matching formula, the SPP$_{1m}$ eigenmode can be effectively phase-matched to the tapered-fibre eigenmode by increasing the relative gap width. We also note that the diameter of the tapered fibre can be optimized to phase-match the cavity eigenmodes to the fibre eigenmode because the fibre diameter determines the mode index of the fibre eigenmode.

The calculated cavity $Q$ factors for SPP$_{1m}$ eigenmodes as a function of azimuthal mode number, $m$, are plotted in Fig. 2c. The error bounds for the imaginary part of the permittivity of silver are taken into account in estimating the bounds on the theoretical $Q$ factors and are discussed in Supplementary Information[24]. The calculated $Q$ factors consist of contributions from intrinsic metal loss (silica material loss is negligible in comparison with metal loss[22,24,25]) and the geometry- and material-dependent radiation loss into free space: $Q^{-1} \approx Q^{-1}_{metal} + Q^{-1}_{rad}$. Therefore, this $Q$ value provides the ideal theoretical limit on the $Q$ performance of SPP microdisk resonators that have negligible scattering loss induced by surface roughness. The radiation-limited $Q$ factor, $Q_{rad}$, is orders of magnitude larger than the metal-loss-limited $Q$ factor, $Q_{metal}$; the ideal SPP microcavity is thus metal-loss limited (see Methods): $Q^{-1} \approx Q^{-1}_{metal}$. In Fig. 2c, the highest fundamental SPP $Q$ factor is found to be 1,800, at the resonant wavelength of 1,062.45 nm ($m = 85$). At a wavelength of 1,568.25 nm ($m = 54$), which is close to the value used in measurements described below (series 1 in Fig. 3), the theoretical $Q$ factor is 1,140 (see Supplementary Information for the lower and upper bounds, $Q_l = 700$ and $Q_u = 2{,}210$). The cavity mode volume, $V$, and the figure of merit $Q/V$ of the SPP microcavity are estimated in Supplementary Information.

To measure the SPP microdisk resonances experimentally, a narrow-linewidth (<300 kHz) tunable external-cavity semiconductor laser is coupled to the tapered fibre waveguide and scanned over the 1,520–1,570-nm wavelength range. The position of the tapered fibre with respect to the SPP microdisk resonator is controlled at a fixed vertical distance by piezoelectric stages with an encoded resolution of 100 nm, and the laser polarization is controlled using a fibre polarization controller and monitored with a polarimeter. For large overlap between the cavity and the waveguide modes, the tapered fibre is positioned underneath the bevelled edge of the resonator, where the silica microdisk is free of silver coating. The output transmission is recorded using a photodetector and a digital oscilloscope. Figure 3a shows the normalized transmission spectrum from an SPP microdisk resonator with a Lorentzian line-shape fit (Fig. 3a, red curve) to each resonance. Two resonances, located at 1,523.59 and 1,532.76 nm ($SPP_{1,83}$ and $DE_{1,74}$, as estimated by calculation), can be clearly identified. An expanded view of the scan (main panel modes outlined) is shown in the inset of Fig. 3a

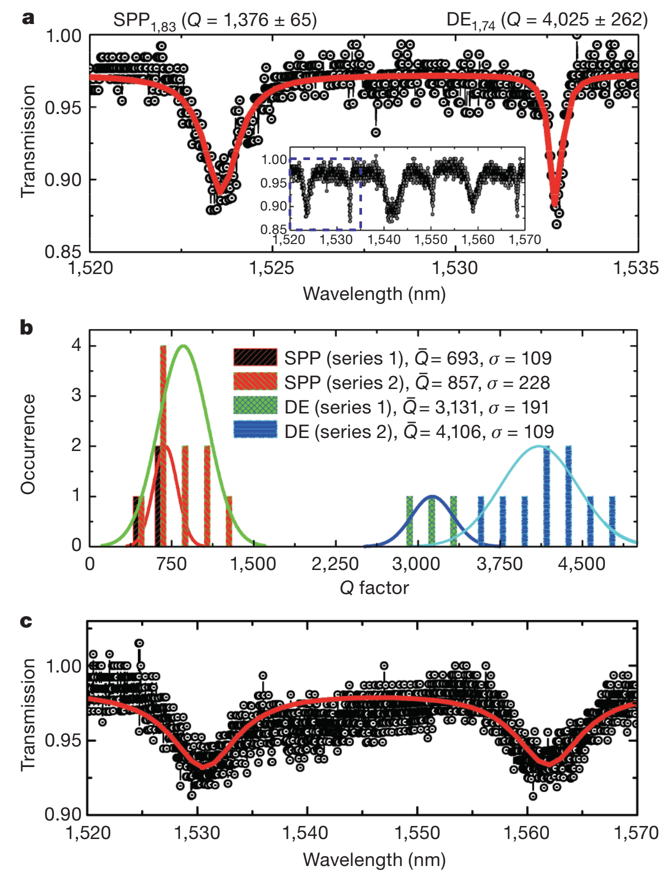


**Figure 3 | *Q*-factor measurements for silver-coated and chromium-coated microdisk resonators.** **a**, Normalized transmission spectrum showing the highest measured SPP $Q$ factor of 1,376 ± 65 and a dielectric resonance with a $Q$ factor of 4,025 ± 262. The inset (main panel outlined) is the entire wavelength band (1,520–1,570 nm) scanned for this sample. $R_b = 15.45 \pm 0.05\ \mu m$, $R_t = 12.73 \pm 0.04\ \mu m$, $d = 2\ \mu m$, $t \approx 100$ nm. **b**, Statistical histogram of measured $Q$ values showing the occurrence of each eigenmode (SPP and dielectric) for two different sample batches (series 1 and series 2). Mean ($\bar{Q}$) and standard deviation ($\sigma$) of $Q$ factors are shown in the key (series 1, $n = 3$ measurements; series 2, $n = 9$). **c**, Normalized transmission spectrum for a chromium-coated microdisk resonator ($R_b \approx 11\ \mu m$, $R_t \approx 7.9\ \mu m$, $d = 2\ \mu m$) with a two-dip Lorentzian fit.

and spans three free spectral ranges of SPP and dielectric eigenmodes. The cavity $Q$ factor for the fundamental $SPP_{1,83}$ eigenmode is found to be 1,376 ± 65 (which falls within the theoretical $Q$-factor range of $760 \lesssim Q \lesssim 2{,}360$, with a nominal $Q$ factor of 1,225 for the $SPP_{1,83}$ eigenmode), and that of the fundamental $DE_{1,74}$ mode is 4,025 ± 262. This SPP $Q$ factor of ~1,376 is over 30 times larger than the $Q$ factors reported in previous SPP cavity work[12–16].

To determine the reproducibility of this $Q$ factor, two series of samples of different nominal sizes (series 1, $R_b = 10.93\ \mu m$; series 2, $R_b = 15.56\ \mu m$) were tested. The measured $Q$ factors for both the SPP and dielectric eigenmodes in the 1,550-nm wavelength band are plotted statistically in Fig. 3b. Two separate clusters of $Q$ factors are seen in this plot, indicating the distinctive resonant characteristics of the two sorts of eigenmode and a tendency for loss to decrease ($Q$ factor to increase) as the size of the cavity increases. The measured $Q$ factors are bounded within the range predicted for the plasmonic eigenmode (see Supplementary Information). To test the metal-dependent resonance characteristics of the SPP microdisk, chromium (which is highly lossy at optical frequencies) was deposited onto the silica microdisk using the same sputtering process, for use in control experiments. The normalized transmission spectrum for a chromium-coated microdisk resonator is shown in Fig. 3c. In this case, only low-$Q$ resonances (for example $Q \approx 213$ at 1,561.92 nm) are observed, owing to the presence of the chromium layer. These resonances are primarily of optical dielectric origin, as confirmed by finite-element simulations, because the fundamental SPP eigenmodes of a chromium-coated microdisk of this size should have a theoretical $Q$ factor of ~10 in the 1,550-nm band.

To verify the phase-matched excitation of the cavity eigenmodes, a series of measurements were performed with variations in the position of the tapered fibre waveguide relative to the SPP cavity. Figure 4 shows the normalized transmission spectra (for an SPP microdisk from a batch from series 2) excited at different gap widths, $d_g$, and also the corresponding optical micrographs and relative positions between the cavity and the tapered fibre waveguide. Each of the eigenmodes is assigned a mode number (Fig. 4a) inferred from finite-element simulations (Methods). The importance of the phase matching between cavity and fibre eigenmodes is manifest in the observed transmission spectra. At larger gap widths ($d_g \approx 0.8, 0.4\ \mu m$), only the resonances of the first- and second-order SPP eigenmodes ($SPP_{1m}$ and $SPP_{2m}$) are observable, and the fundamental dielectric eigenmode ($DE_{1m}$) resonances are absent. This is because, for this range of larger gap widths, SPP eigenmodes are better phase-matched to the fibre eigenmode[26] and have a larger field overlap with the fundamental fibre eigenmode (they are located closer to the edge of, and extend farther outside, the microcavity than does the fundamental dielectric eigenmode in the wedge-shaped structure). As the gap width decreases further ($d_g \leq 0$), the fundamental dielectric eigenmodes are excited, as the phase-matching condition can be partly satisfied by decreasing $d_g$. For negative gap width, the SPP resonances are even more pronounced, as the phase-matching condition between the SPP and fibre eigenmodes can be fully satisfied owing to gap-width-induced phase matching, as is shown qualitatively in Fig. 2b. For the SPP resonance at 1565.4 nm, an input power transfer of up to 49.7% is demonstrated, showing the effectiveness of phase-matching control using the tapered fibre waveguide.

The demonstration of high-$Q$ surface-plasmonic microcavities opens many possibilities for applications in fields ranging from fundamental science to device engineering. As a specific example, it could make possible a plasmonic laser, for which adequate gain materials as well as a high-$Q$ SPP cavity are key prerequisites[27]. Although the demonstrated SPP $Q$ factor is still less than that of an optical micro- or nanocavity[10,11], the corresponding SPP loss coefficient of $\alpha_{SPP} \approx 2\pi n_c/\lambda Q_{SPP} \approx 39\ cm^{-1}$ (where $\lambda$ is the wavelength) satisfies the experimental criteria for a laser cavity and shows that, in principle, such surface-plasmonic lasing devices are possible. The tapered-fibre excitation scheme also demonstrates a convenient means of exciting these structures and selectively probing SPP cavity modes, because it directly controls the mode overlap and phase matching between the cavity and fibre eigenmodes (we also note

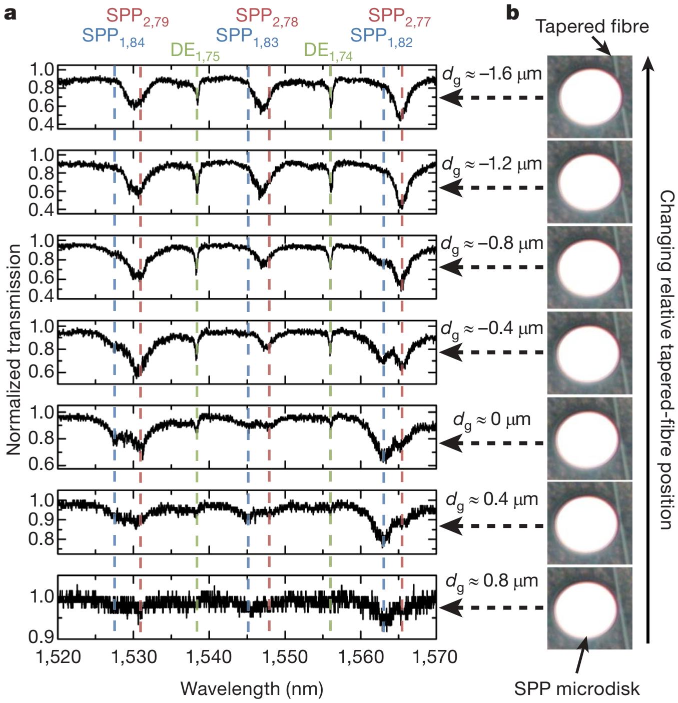


**Figure 4 | Transmission spectrum versus waveguide coupling gap. a,** Series of normalized transmission spectra, recorded for a variety of gap widths between the tapered fibre waveguide and the edge of the SPP microdisk. Resonances of SPP and dielectric eigenmodes are shown with estimated mode numbers. $R_b = 15.70 \pm 0.185$ μm, $R_t = 13.08 \pm 0.14$ μm, $d = 2$ μm, $t \approx 100$ nm. For the SPP resonance at 1565.4 nm, an input power transfer of up to 49.7% is demonstrated (second panel from the top). **b,** Optical micrographs corresponding to the recorded normalized transmission spectra. Estimated gap width, $d_g$, is also shown.

that coupling to a conventional, chip-based waveguide is possible[28]). Furthermore, it is notable that the SPP $Q$ factor could be substantially increased beyond the values measured here by lowering the temperature of the SPP microcavity[27,29]. From a fundamental standpoint, the SPP $Q$ factor is sufficient to observe interesting cavity quantum electrodynamical phenomena in the weak-coupling regime relating to enhanced Purcell factors[11,29,30]. In addition, using the high nonlinearity of metal (or materials deposited in the vicinity of the metal), it may be possible to extend the applications of nonlinear plasmonics. Finally, it should be noted that, because the $\lambda^3 Q/V$ values of the present SPP microcavity (approximately a few hundred) are still much less than those provided by the photonic-crystal and dielectric whispering-gallery microcavities[10,11], it is still important to pursue new plasmonic cavity designs.

## METHODS SUMMARY

**Fabrication of SPP microdisk resonators.** The template silica microdisks are fabricated by photolithography and buffered oxide etching as described elsewhere[19,21]. During the wet etch, the photoresist is undercut and produces a bevelled silica edge, which provides conformal silver coating of the top surface of the microdisk. The silver coating is deposited on the template silica microdisks using a d.c. sputtering technique with a chamber argon pressure of 30 mtorr. Two batches of samples (series 1 and 2) are prepared in this way to investigate the size-dependent characteristics of SPP microcavities.

**Phase-matching condition.** An asymptotic phase-matching formula can be obtained by two different approaches. Using the coupled-mode theory, the evaluation of the coupling coefficient $\kappa$ involves the overlap integral of the cavity eigenmode and the tapered-fibre eigenmode. To have a non-zero coupling strength, the waveguide mode index can be approximated as written in equation (1) by setting the $\phi$ dependence of the integrand to zero. The same phase-matching condition can be found by path-averaging the effective mode index seen by the straight fibre waveguide[26]. This gives exactly the same formula

$$n_w \approx n_c \frac{2\tan^{-1}\left(\delta/\sqrt{\delta(2-\delta)}\right)}{\sqrt{\delta(2-\delta)}} = n_c\left(1+\frac{1}{3}\delta+\frac{2}{15}\delta^2+O(\delta^3)\right)$$

confirming the asymptotic dependence of phase matching on the relative gap width, $\delta$. This formula applies only to the case of negative gap width, that is, $\delta = -d_g/R_b \geq 0$.

**Full Methods** and any associated references are available in the online version of the paper at www.nature.com/nature.

**Received 12 July; accepted 6 November 2008.**

1. Raether, H. R. *Surface Plasmons on Smooth and Rough Surfaces and on Gratings* (Springer, 1988).
2. Barnes, W. L., Dereux, A. & Ebbesen, T. W. Surface plasmon subwavelength optics. *Nature* **424,** 824–830 (2003).
3. Maier, S. A. *et al.* Local detection of electromagnetic energy transport below the diffraction limit in metal nanoparticle plasmon waveguides. *Nature Mater.* **2,** 229–232 (2003).
4. Stockman, M. I. Nanofocusing of optical energy in tapered plasmonic waveguides. *Phys. Rev. Lett.* **93,** 137404 (2004).
5. Ozbay, E. Plasmonics: Merging photonics and electronics at nanoscale dimensions. *Science* **311,** 189–193 (2006).
6. Cubukcu, E., Kort, E. A., Crozier, K. B. & Capasso, F. Plasmonic laser antenna. *Appl. Phys. Lett.* **89,** 093120 (2006).
7. Lopez-Tejeira, F. *et al.* Efficient unidirectional nanoslit couplers for surface plasmons. *Nature Phys.* **3,** 324–328 (2007).
8. Lal, S., Link, S. & Halas, N. J. Nano-optics from sensing to waveguiding. *Nature Photon.* **1,** 641–648 (2007).
9. Brongersma, M. L. & Kik, P. G. *Surface Plasmon Nanophotonics* (Springer, 2007).
10. Vahala, K. J. Optical microcavities. *Nature* **424,** 839–846 (2003).
11. Noda, S., Fujita, M. & Asano, T. Spontaneous-emission control by photonic crystals and nanocavities. *Nature Photon.* **1,** 449–458 (2007).
12. Ditlbacher, H. *et al.* Silver nanowires as surface plasmon resonators. *Phys. Rev. Lett.* **95,** 257403 (2005).
13. Bozhevolnyi, S. I., Volkov, V. S., Devaux, E., Laluet, J.-Y. & Ebbesen, T. W. Channel plasmon subwavelength waveguide components including interferometers and ring resonators. *Nature* **440,** 508–511 (2006).
14. Miyazaki, H. T. & Kurokawa, Y. Squeezing visible light waves into a 3-nm-thick and 55-nm-long plasmon cavity. *Phys. Rev. Lett.* **96,** 097401 (2006).
15. Weeber, J.-C., Bouhelier, A., Colas des Francs, G., Markey, L. & Dereux, A. Submicrometer in-plane integrated surface plasmon cavities. *Nano Lett.* **7,** 1352–1359 (2007).
16. Vesseur, E. J. R. *et al.* Surface plasmon polariton modes in a single-crystal Au nanoresonator fabricated using focused-ion-beam milling. *Appl. Phys. Lett.* **92,** 083110 (2008).
17. Cai, M., Painter, O. & Vahala, K. J. Observation of critical coupling in a fiber taper to a silica-microsphere whispering-gallery mode system. *Phys. Rev. Lett.* **85,** 74–77 (2000).
18. Spillane, S. M., Kippenberg, T. J., Painter, O. J. & Vahala, K. J. Ideality in a fiber-taper-coupled microresonator system for application to cavity quantum electrodynamics. *Phys. Rev. Lett.* **91,** 043902 (2003).
19. Kippenberg, T. J., Kalkman, J., Polman, A. & Vahala, K. J. Demonstration of an erbium-doped microdisk laser on a silicon chip. *Phys. Rev. A* **74,** 051802(R) (2006).
20. Borselli, M., Johnson, T. J. & Painter, O. Beyond the Rayleigh scattering limit in high-*Q* silicon microdisks: theory and experiment. *Opt. Express* **13,** 1515–1530 (2005).
21. Armani, D. K., Kippenberg, T. J., Spillane, S. M. & Vahala, K. J. Ultra-high-*Q* toroid microcavity on a chip. *Nature* **421,** 925–929 (2003).
22. Spillane, S. *et al.* Ultra-high-*Q* toroidal microcavities for cavity quantum electrodynamics. *Phys. Rev. A* **71,** 013817 (2005).
23. Oxborrow, M. Traceable 2-D finite-element simulation of the whispering-gallery modes of axisymmetric electromagnetic resonators. *IEEE Trans. Microw. Theory Tech.* **55,** 1209–1218 (2007).
24. Johnson, P. B. & Christy, R. W. Optical constants of noble metals. *Phys. Rev. B* **6,** 4370–4379 (1972).
25. Palik, E. D. *Handbook of Optical Constants of Solids* (Academic, 1985).
26. Rowland, D. R. & Love, J. D. Evanescent wave coupling of whispering gallery modes of a dielectric cylinder. *IEE Proc. J. Optoelectron.* **140,** 177–188 (1993).
27. Hill, M. T. *et al.* Lasing in metallic-coated nanocavities. *Nature Photon.* **1,** 589–594 (2007).
28. Almeida, V. R., Barrios, C. A., Panepucci, R. R. & Lipson, M. All-optical control of light on a silicon chip. *Nature* **431,** 1081–1084 (2004).
29. Gong, Y. Y. & Vučković, J. Design of plasmon cavities for solid-state cavity quantum electrodynamics applications. *Appl. Phys. Lett.* **90,** 033113 (2007).
30. Akimov, A. V. *et al.* Generation of single optical plasmons in metallic nanowires coupled to quantum dots. *Nature* **450,** 402–406 (2007).

**Supplementary Information** is linked to the online version of the paper at www.nature.com/nature.

**Acknowledgements** We thank R. F. Oulton and G. Bartal for discussions and S. Zhang for a critical reading of the manuscript. This work was supported by the US Air Force Office of Scientific Research MURI program (grant no. FA9550-04-1-0434) and by the NSF Nanoscale Science and Engineering Center under award no. DMI-0327077.

**Author Information** Reprints and permissions information is available at www.nature.com/reprints. Correspondence and requests for materials should be addressed to X.Z. (xiang@berkeley.edu) or K.V. (vahala@caltech.edu).

doi:10.1038/nature07627 

## METHODS

**Mode number of a dielectric eigenmode.** The mode numbers, $h = 1, 2, \ldots$, of the dielectric eigenmodes $DE_{hm}$ are assigned in order from lowest- to highest-order dielectric eigenmode. Depending on the geometry and the mode number $h$, dielectric eigenmodes can possess certain degrees of plasmonic characteristics due to the presence of the metal–silica interface.

**Theoretical *Q*-factor estimation.** From the finite-element eigenfrequency analysis, the complex-valued eigenfrequency, $f = f_{re} + if_{im}$, can be calculated, and $Q$ factors evaluated using the formula $Q = f_{re}/2f_{im}$. The ranges of theoretical $Q$ factors are estimated by using the error bounds in the imaginary part of the permittivity of silver. The radiation-limited $Q$ factor can be estimated and separated from the metal-loss-limited $Q$ factor by removing the imaginary part of the permittivity of silver. For example, the radiation-limited $Q$ factor for $m = 54$ (Fig. 2c) is $3.9 \times 10^6$, and for $m = 85$ the $Q$ factor is $6.7 \times 10^9$, both of which are orders of magnitude larger than the total $Q$ factors.

**Eigenmode identification.** To assign mode numbers to the experimentally obtained resonance spectra, such as those shown in Fig. 4a, the size of the cavity is measured with a scanning electron microscope and the measured geometrical dimension is used in the finite-element calculation. Owing to the high sensitivity of the resonance frequency with respect to the nanoscale geometrical variation and the permittivity of the component materials, only the approximate mode numbers can be inferred. There being distinct ranges of $Q$ factors indirectly confirms the theoretical SPP and dielectric resonance locations. Then the transmission of each resonance is experimentally determined by varying the gap width and the input polarization to assign distinct resonant characteristics precisely to each of the eigenmodes.